Development of Mudulus: A Muography Detector Based on Double-Synchronized Electronics for Geophysical Applications

R. Calderón-Ardila,[1,2] H. Asorey,[1,2,3] A. Almela,[1,4] A. Sedoski,[1] C. Varela,[1] N. Leal,[1] and M. Gomez-Berisso[3] for the MuAr group

[1]*Instituto de Tecnologías en Detección y Astropartículas, (CNEA-CONICET-UNSAM), Buenos Aires, Argentina*
[2]*Instituto SABATO, Universidad Nacional de San Martín, Centro Atómico Constituyentes, Buenos Aires, Argentina*
[3]*Instituto Balseiro (CAB-CNEA) and Universidad Nacional de Cuyo, San Carlos de Bariloche, Argentina*
[4]*Universidad Tecnólogica Nacional, Facultad Regional Buenos Aires, Argentina*

Corresponding author: R. Calderón-Ardila
Email: rolando.calderon@iteda.cnea.gov.ar

Abstract

In this paper, we present a prototype modular muon detector ("Mudulus"), based on our previous experience with the design of the MuTe detector in Colombia and the AMIGA buried muon detectors in the Pierre Auger Collaboration. Our group is developing detectors for muography and multipurpose applications. Our prototype detectors use different modules of plastic scintillators with embedded optical fibers and 64 channel multianode photomultiplier tubes (PMTs) with a common dynode or arrays of Silicon Photomultipliers (SiPM). In the case of Mudulus, each module is made of 12 scintillator strips of $(4 \times 1 \times 100)\,\mathrm{cm}^3$ coupled with a lengthwise running Wavelength Shifter (WLS) fiber, connected at each end to a PMT channel. This design allows us to build panels with up to four of these modules. This modular configuration allows changing the panel geometries looking for an adaptive shape or size to the studied object and resulting in a detailed muography image. The improvement in performance obtained with Mudulus is achieved by the combination of its modular design and the double-synchronized detection at the end of each scintillator bar. We take advantage of measuring at both ends of each strip to determine the muon flux using a model to account for signal attenuation in each anode, and then determine the position of the incoming muons with better discrimination and subpixel spatial resolution.

Keywords: muography, geophysics, astroparticle techniques, geophysical imaging
DOI: 10.31526/JAIS.2022.300

1. INTRODUCTION

Muography is a technique that allows constructing an image of the inner mass density distribution of an object due to the difference in absorption of atmospheric muons as they pass through a target. Muons ($\mu^{\pm}$) are used for tomography techniques because of their great penetration power due to low interaction with matter [1]. Moreover, muon flux is relatively constant, natural, abundant, and free to use. Additionally, muons are produced in Earth's atmosphere with known angular and energy distributions, with a flux of $\sim 1\,\mu^{\pm}/(\mathrm{cm}^2 \times \mathrm{minute})$ at sea level, and can traverse through large thicknesses of rock (up to kilometer [12]). The differential flux of incident cosmic muons is usually given in $\mathrm{cm}^{-2}\,\mathrm{sr}^{-1}\,\mathrm{s}^{-1}\,\mathrm{GeV}^{-1}$ and depends on the measurement site and zenith angles. This technique is used for applications that require a noninvasive study. It is used in different fields like archaeology [13, 14, 15], civil engineering [16, 17], nuclear safety [18], and geosciences. For this last one, several applications have been proposed, such as prospecting [19, 20], imaging of underground structures [17], and volcano muography [12, 21]. In Latin America, detectors have been developed for similar purposes in Mexico [4], Colombia [5, 6, 8], and Argentina [9] and are also currently under development in Peru.

This work focuses on the development of modular panels for muography applications. Our overall module design aims to produce easy-to-transport modules, with the capability of improving the resolution of the resulting image. This is done by taking advantage of a synchronized measurement of the attenuation of the light along the optical fibers.

Muography requires an instrument capable of counting muons. The accuracy of the obtained images depends mainly on the effective measurement area, spatial resolution, and exposure time [2]. Our detector is composed of plastic, rectangular-shaped scintillator bars. These materials allow the detection of muons by producing light when a charged particle passes through them. The average energy deposited by a muon on a plastic scintillator strip is around $\sim 2\,\mathrm{MeV} \times \mathrm{cm}^{-1}$ [7], and the scintillator strips used for our modules generate one optical photon for every 100 eV of deposited energy [3].

This work is motivated by the search for possible improvement of the spatial resolution of plastic scintillator detectors [10] via synchronized double detection using multichannel PMTs. Our goal is to build modular detectors capable of imaging geophysical

and other large structures. This work is the result of technology transfer from the AMIGA (Auger Muons and Infill for the Ground Array) project [11] at the Pierre Auger Observatory in Malargüe, Argentina.

2. SCINTILLATOR DETECTOR PROTOTYPE

Mudulus consists of four scintillator modules covering a total area of 1 m^2. Each panel has 12 plastic scintillator strips measuring 100 cm in length, 4.1 cm in width, and 1 cm in height. Each scintillator strip in these modules is coupled lengthwise with a wavelength-shifting (WLS) optical fiber. Both ends of each fiber are coupled to a channel of a multianode PMT (one PMT for each end). The outputs of each PMT are connected to a front-end electronics board that digitizes the anode pulses using comparators and digitizes the dynode pulses using a 14-bit Analog to Digital Converter (ADC). Each comparator has an individually set threshold level, used to set the operating point of its PMT channel.

A data acquisition system samples and analyzes all outputs of the front-end electronics, storing the traces of possible muons as determined by the online analysis. These traces are then stored in a data storage system and have an offline analysis to determine if they are effectively muon traces and, in that case, to reconstruct the position within the scintillators of the impinging muon. This detector must be calibrated before any measurements can be taken. The calibration procedure consists of finding and setting the operating point for each acquisition electronics and is described in Section 3. After calibrating each acquisition electronics, a two-dimensional projection image from the scintillator telescope can be obtained.

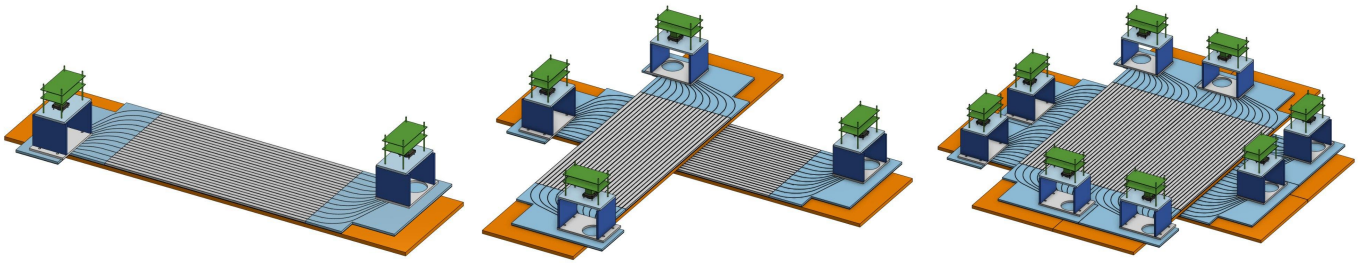

(a) One module (b) Two modules (c) Panel - four modules

FIGURE 1: Prototype design. (a) One module. (b) Two crossed panels with 12 scintillator strips resulting in $(12 \times 12 = 144)$ pixels with $\sim$0.25 m^2 of effective detection area (left). (c) Using four panels, it is possible to generate $(24 \times 24 = 576)$ pixels with a total detection area of $\sim$1 m^2. Every panel could have up to one synchronized detection electronics at each end. The modular design allows changes to the spatial configuration and the detector resolution.

2.1. Modular Detector Prototype

The prototype is built with a structure assembled with a PVC casing. The casing contains 12 plastic scintillator strips doped with 1% of PPO [2,5-diphenyloxazole] and 0.03% of POPOP [1,4-bis(5-phenyloxazole-2-yl) benzene], with a TiO_2 coating [22]. Each scintillator strip is coupled with an optical WLS fiber (Saint-Gobain BCF99-29AMC) that runs lengthwise throughout the entire strip. These fibers have a diameter of 1.2 mm with a length of 2 m. They shift in wavelength the photons produced in the scintillator (from blue/UV light to green light) and transport the green photons lengthwise. The attenuation lengths in the scintillator bars are $\sim$5 cm for the fast component and $\sim$24 cm for the slow component. Given these short attenuation lengths, fibers are necessary for transporting the produced light to the PMTs.

Each panel uses two multianode PMTs (Hamamatsu H8804-200MOD) as shown in Figure 2(c). Each PMT photocathode is coupled with 12 WLS fibers in a pattern that guarantees a minimum spacing of one uncoupled PMT channel in every direction from a coupled channel to minimize optical crosstalk noise. The coupling of these fibers with the PMT is achieved using a mechanical coupling device ("cookie") made of plastic material of Polyoxymethylene (POM). All fibers are glued to this cookie using optical cement, and the cookie provides mounting points to hold the PMT in place.

2.2. Synchronization

Synchronization with the prototype electronics is achieved with a modified AMIGA BackEnd board [11] that provides a synchronization signal (Pulse Per Second, PPS). This PPS contains the UNIX timestamp of the sending electronics and is sent periodically via SPI. The data acquisition electronics read this PPS and use the received value as part of the event identifier, resetting all internal clocks used for event tagging upon receiving the signal.

2.3. The Acquisition System

The acquisition system consists of three main parts: A front-end, represented in Figure 3 in blue lines, which receives signals from the 12 active PMT channels; a digital readout based on an Altera Cyclone III Field-Programmable Gate Array (FPGA) with a sampling rate of 320 Msps; and a control system, consisting of a low-power computer where the configuration, monitoring, and

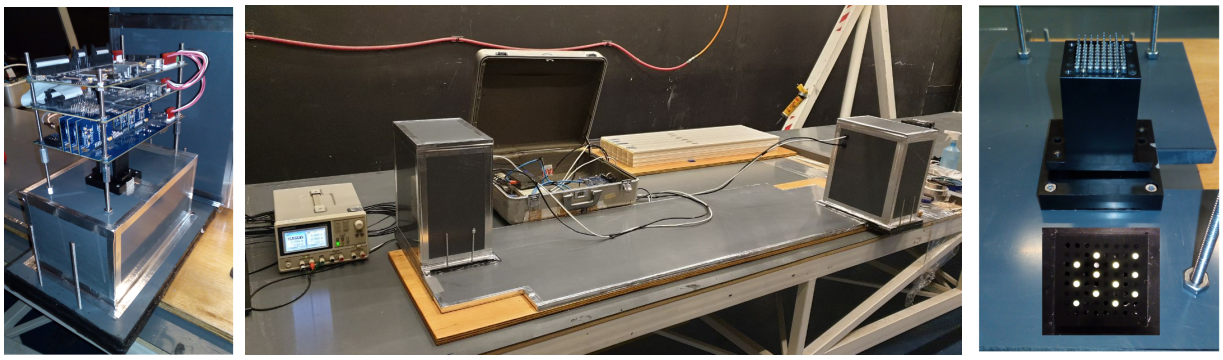

(a) Readout electronics (b) Module (c) PMT and coupling

FIGURE 2: (a) Digitization and acquisition electronics using PMT. (b) Image of a prototype detector module, showing the eKit in dark boxes at the ends of the array of 12 scintillator strips. (c) Image of a PMT standing on top of a cookie (top). The cookie has 12 fibers distributed to avoid optical crosstalk (bottom).

communication programs are run on a Linux operating system. The dynode uses a 14-bit ADC that digitizes the signal from the dynode sampling at 160 Msps.

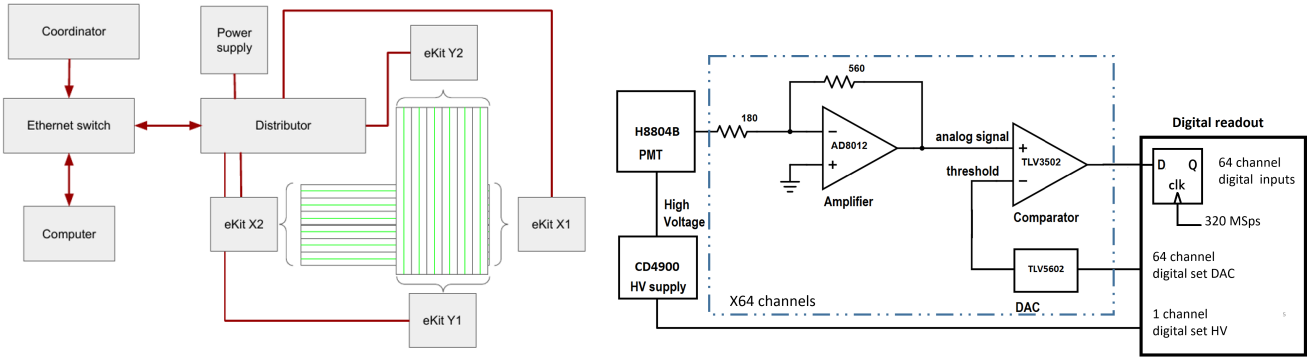

(a) Communication diagram (b) Data acquisition electronic system

FIGURE 3: (a) Diagram of the electronics and detector. Each eKit consists of the acquisition electronics, a mechanical coupling, and a PMT. The Ethernet switch creates an Ethernet LAN. The distributor replicates the synchronization signal and provides power to the electronics kits. (b) Diagram of the electronics acquisition system.

3. CALIBRATION AND DATA ACQUISITION

The objective of this detector is to count muons in different configurations and arrangements; see Figure 1 to reconstruct images. First, it is necessary to calibrate the PMTs, estimate the equivalence for (single photo-electron, SPE) in mode analog (charge), and calibrate in digital mode by determining the operating voltage and the appropriate thresholds for each channel. The synchronization of two AMIGA electronics kits (eKits) [10] per panel reduces false positives. It also allows locating an event within the target thanks to calibration with a reference distance [23]. In addition, we seek to reach subpixel resolution measurements ($\leq$4 cm) using the PMT dynode.

To calibrate the eKit, the front-end digitizes the signal through a discriminator, which would correspond to a one-bit ADC, and changes the state depending on whether the trace exceeds the threshold. The calibration of an eKit is a two-stage process: first, we obtain the operating point of the HV power supply; with an HV voltage set, we then obtain the operating point for each comparator. We use an analytical method to obtain the calibration parameters of the PMT by employing a discriminator and sweeping the threshold to study the response. We use an analytical method to analyze the data from both calibration runs.

This procedure is as follows. To obtain the HV operating point, we set the comparator threshold for all PMT channels to 20 mV; then, we vary the polarization voltage from -600 V to -1000 V in steps of -10 V; see Figure 4(b) measuring the pulse rate for each step during 120 s. After these measurements, we obtain, by adjusting the pulse rate measurement, the optimal operating voltage point for each channel. The final polarization voltage is selected as the optimal polarization for the channel with the lowest gain.

Once the operating voltage has been set, we obtain the survival function for all PMT channels by sweeping the comparator thresholds: from 10 mV to 800 mV in 10 mV increments, measuring for 240 s for each step [11]. Finally, we fit the survival functions

for each channel using a PMT response model to obtain the curve parameter, and set the threshold of each channel at 30% of its SPE peak.

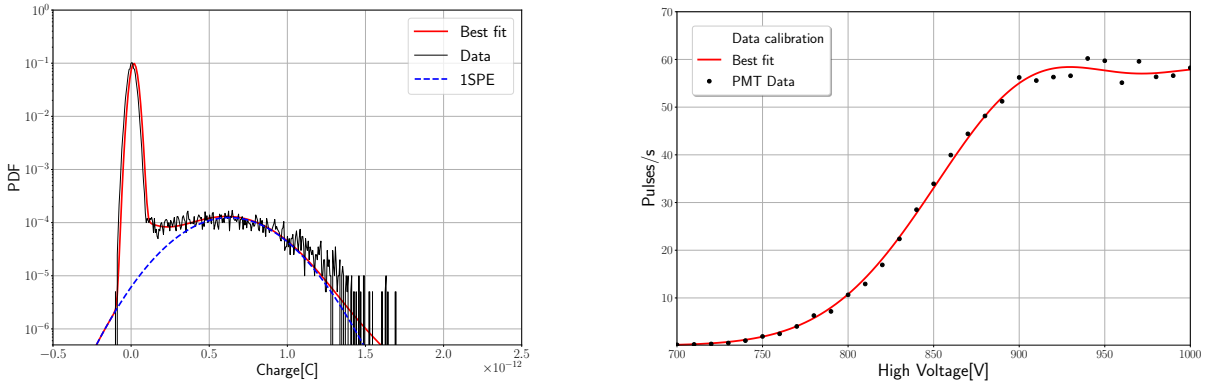

(a) Analog calibration for PMT

(b) Digital calibration in HV for PMT channels

FIGURE 4: (a) From analogical pulses, we determined a calibration histogram. For each anode, the pulse amplitude is proportional to the number of impinging photons on the photocathode. The plot contains two peaks: the first (left) peak represents the most likely charge value for background noise, while the second (right) peak represents the average charge for one (single photoelectron, SPE). (b) For optimal PMT performance, a digital calibration is also performed to determine the bias voltage for each channel.

4. SUMMARY AND OUTLOOK

In this paper, we present the progress in the prototype development of a modular muon detector based on plastic scintillators and PMTs. Additionally, the design proposes performing synchronized detection for each scintillator bar; this will help in background studies and will allow obtaining subpixel resolution through the dynode. We currently have the acquisition system and four complete module prototypes; we are calibrating the prototype detectors to perform muography imaging in geophysical targets.

CONFLICTS OF INTEREST

The authors declare that there are no conflicts of interest regarding the publication of this paper.

ACKNOWLEDGMENTS

The authors are very thankful to the participating institutions. They would like to thank the National Scientific and Technical Research Council (CONICET) and the Pierre Auger Collaboration for their support and M. Hampel, A. Fuster, A. Riello, N. Del Castillo, M. Platino, and G. Pierri for their support.

References

[1] E. V. Bugaev et al., Phys. Rev. C **58**, 054001 (1998).
[2] L. Bonechi et al., Rev. in Phys. **5**, 100038 (2020).
[3] Z. W. Bell, Handbook of Part. Det. and Imag. **Vol2**, Ch15-370 (2012).
[4] A. Menchaca-Rocha et al., PoS (X LASNPA) **194** 012 (2014).
[5] A. Vesga-Ramírez et al., Ann. Geophys. **63** 661 (2020).
[6] J. Peña-Rodríguez et al., JINST **15** P09006 (2020).
[7] A. Vásquez-Ramírez et al., JINST **15** P08004 (2020).
[8] A. Vesga-Ramírez et al., SAMES **109** 103248 (2021).
[9] R. Calderón-Ardila et al., ESSOAr AGU2020 (2021).
[10] M. Platino et al., JINST **06** P06006 (2011).
[11] A. Aab et al. [Pierre Auger Coll.], JINST **11** P02012 (2016).
[12] N. Lesparre et al., Geophys. J. Int. **183** 1348–1361 (2010).
[13] L. W. Alvarez et al., Science **167** 832–839 (1970).
[14] M. Menichelli et al., Nucl. Instrum. and Meth. in Phys. A **572** 262–265 (2007).
[15] K. Morishima et al., Nature **552** 386–390 (2017).
[16] E. Guardincerri et al., CAIP Advances **06** 015213 (2016).
[17] G. Saracino et al., Phil. Trans. R. Soc. A. **377** 20180057 (2019).

[18] D. Mahon et al., Phil. Trans. R. Soc. A. **377** 20180048 (2019).
[19] D. Schouten., Phil. Trans. R. Soc. A. **377** 20180061 (2019).
[20] A. Bonneville et al., Phil. Trans. R. Soc. A. **377** 20180060 (2019).
[21] H. Tanaka., Phil. Trans. R. Soc. A. **377** 20180142 (2019).
[22] A. Pla-Dalmau et al., Nucl. Instrum. and Meth. in Phys. A **466** 482–491 (2001).
[23] R. Calderón-Ardila et al., preprint arXiv:2006.03165 (2020).